particles

IMPACT FACTOR 2.3

CITESCORE 3.0

Article

Production Optimization of Exotic Hypernuclei via Heavy-Ion Beams at GSI-FAIR

Samuel Escrig and Christophe Rappold

Special Issue

Selected Papers from the 4th MODE Workshop on Differentiable Programming for Experiment Design

Edited by

Prof. Dr. Tommaso Dorigo, Dr. Roberto Ruiz de Austri Bazan, Prof. Dr. Jose Salt and Dr. Pietro Vischia

MDPI

https://doi.org/10.3390/particles8020054

particles

MDPI

Article

Production Optimization of Exotic Hypernuclei via Heavy-Ion Beams at GSI-FAIR

Samuel Escrig * and Christophe Rappold

Instituto de Estructura de la Materia (IEM-CSIC), 28006 Madrid, Spain; christophe.rappold@csic.es
* Correspondence: samuel.escrig@csic.es

Abstract: Building on the successful demonstration of hypernuclear spectroscopy using heavy-ion beams, the HypHI Collaboration is shifting its focus to investigating proton- and neutron-rich hypernuclei. A crucial component of this research is the implementation of a fragment separator, which facilitates the production and separation of rare isotope beams and is vital for accessing hypernuclei far from the stability line. High-precision spectroscopy of these exotic hypernuclei is planned to be conducted at GSI first, which will be followed by experiments at the FAIR facility utilizing the FRS and Super-FRS fragment separators. A thorough systematic investigation paired with an optimization analysis was employed to establish the most favorable experimental setup for producing high-isospin hypernuclei. Theoretical models describing heavy-ion-induced reactions and hypernuclear synthesis guided this process, which was complemented by Monte Carlo simulations to obtain experimental efficiencies for the production and transmission of the exotic secondary beams. The outlined methodology offers insights into the anticipated yields of ${}^{6}_{\Lambda}$He, ${}^{9}_{\Lambda}$C, and a range of both proton- and neutron-rich hypernuclei.

Keywords: exotic hypernuclear spectroscopy; optimal design; heavy-ion-induced reaction; fragment separator

Academic Editors: Tommaso Dorigo, Roberto Ruiz de Austri Bazan, Jose Salt and Pietro Vischia

Received: 28 February 2025
Revised: 30 March 2025
Accepted: 19 April 2025
Published: 1 May 2025

Citation: Escrig, S.; Rappold, C. Production Optimization of Exotic Hypernuclei via Heavy-Ion Beams at GSI-FAIR. *Particles* **2025**, *8*, 54. https://doi.org/10.3390/particles8020054

1. Introduction

The study of strangeness production in nuclear and hadronic collisions has gained increasing interest over the past few decades. Standard nuclear matter consists of ordinary nucleons, which are formed by triplets of the lightest up and down quarks. However, a deeper understanding of dense matter properties necessitates the inclusion of the strange (s) quark [1,2]. Hypernuclei, which are bound systems containing both nucleons and hyperons (baryons with at least one s-quark), are invaluable for probing hyperon–nucleon and hyperon–hyperon interactions [3].

Since 2006, the HypHI Collaboration has conducted extensive research on hypernuclei at the GSI facility [4]. Moving forward, the forthcoming experiments of the HypHI Collaboration will take place not only at GSI but also at the future GSI-FAIR [5]. The GSI facility currently offers a wide array of ion beams, ranging from protons to uranium, enabled by the 18 Tm heavy-ion synchrotron (SIS18) [6,7], and produces exotic beams using the fragment separator (FRS) [8,9]. The SIS18 synchrotron is capable of delivering ion beams with kinetic energies up to 2 AGeV for nuclei with $A/Z = 2$. The future FAIR facility represents a substantial upgrade, incorporating an additional synchrotron ring with a magnetic rigidity of 100 Tm (SIS100). Various experimental setups are under development at FAIR to support advanced research in nuclear and hadron physics. One of these initiatives, the NUSTAR

program, includes the construction of a superconducting fragment separator (Super-FRS) with a 20 Tm magnetic rigidity, enabling powerful in-flight separation of exotic nuclei [10].

Research activities at HypHI Collaboration have employed a novel experimental method distinct from the conventional missing mass techniques that use meson or electron beams. These traditional approaches are utilized at renowned institutions such as KEK, JPARC, DAΦNE, JLab, and MAMI-C accelerator [11–13]. The production of hypernuclei in the projectile rapidity was first undertaken with ^{16}O beams at 2.1 *A*GeV on a polyethylene target [14]. Subsequently, the hypernucleus production was aimed via the ^{4}He and ^{7}Li beams on a polyethylene target with the respective beam energies of 3.7 *A*GeV and 3.0 *A*GeV [15,16]. The obtained results were not conclusive because of the too small number of observed events.

Notwithstanding, the Phase 0 experiment of HypHI, conducted at GSI in 2009 and 2010, successfully demonstrated the feasibility of high-precision hypernuclear spectroscopy through heavy-ion induced reactions [17–19]. This experiment involved bombarding a stable ^{12}C target with a ^{6}Li beam at 2 *A*GeV, leading to the production and identification of hypernuclei like ${}^{3}_{\Lambda}$H, ${}^{4}_{\Lambda}$H, and ${}^{5}_{\Lambda}$He. These achievements validated the experimental method, which diverges from traditional approaches by enabling the reconstruction and identification of decay vertices of Λ particles in a more inclusive setup.

Due to the experimental setup's open geometry, characteristic of inclusive experiments, several hypernuclear bound states were identified by measuring all possible decay fragments within the same data taking. Furthermore, an indication of a potential new bound state, a neutral hypernucleus formed by two neutrons and a Λ^0 hyperon, was observed when reconstructing the invariant mass of $d + \pi^-$ and $t + \pi^-$ [18]. On the theoretical side, recent calculations have challenged the existence of this ${}^{3}_{\Lambda}$n bound state [20–24], highlighting the need for precise exclusive mass measurements to either confirm or refute this hypothesis.

The Phase 1 experiment, the so-called WASA-FRS HypHI Experiment, aimed at the study of the hypernuclei ${}^{3}_{\Lambda}$H, ${}^{4}_{\Lambda}$H, and nnΛ [25–27]. The primary objectives of this experiment are twofold: to shed light on the hypertriton puzzle and to investigate the existence of the previously proposed nnΛ bound state. Firstly, the significantly shorter hypertriton lifetime reported by three independent state-of-the-art experiments, namely ALICE [28], STAR [29], and HypHI [17], compared to the predictions of theoretical models remains poorly understood. Therefore, obtaining new accurate results for the invariant mass and lifetime of ${}^{3}_{\Lambda}$H (and ${}^{4}_{\Lambda}$H) is crucial to reach a definitive conclusion. Secondly, the observed enhancement in the invariant mass distributions of the $d + \pi^-$ and $t + \pi^-$ final states, as reported by the HypHI Collaboration [18], cannot be accounted for by existing theoretical calculations, which indicate the absence of a neutral nnΛ bound state. Consequently, the WASA-FRS HypHI Experiment aims to produce more precise and statistically significant experimental results that can provide clarification on the potential existence of nnΛ. For this purpose, the distinctive combination of the high-resolution spectrometer FRS [9] and the high-acceptance detector system WASA [30] is used. The hypernuclear production was by means of heavy-ion induced reactions, specifically a beam of ^{6}Li at 2 *A*GeV bombarding a stable ^{12}C target. The experiment was successfully conducted at GSI in 2022 within the Super-FRS Experiment Collaboration. Currently, the data from the experiment are under analysis.

The next phases of the HypHI project are focused on the exploration of exotic hypernuclei approaching the proton and neutron drip lines. This ambitious endeavor will require rare-isotope beams to extend the hypernuclear chart toward proton-rich ${}^{22}_{\Lambda}$Si and neutron-rich ${}^{14}_{\Lambda}$Li hypernuclei. Actually, significant charge symmetry breaking effects are anticipated

in these hypernuclei, potentially altering the drip-line positions due to differences between Λ-proton and Λ-neutron interactions.

The production of exotic hypernuclei can be influenced by the isospin of the beam projectile, as explored in this study. The objective of this investigation was to determine the experimental conditions required for the production of proton-rich or neutron-rich hypernuclei. This article presents a feasibility study demonstrating the potential for operating the Super-FRS at energies around 2 *A*GeV. To achieve the desired exotic hypernucleus, the appropriate primary beam and target isotopes must be selected. The exotic beam generated will then collide with a secondary production target to produce the hypernucleus of interest.

This analysis is an extension of a previous work [31] to new exotic hypernuclei that can be produced and studied with the combination WASA-FRS at GSI.

2. Materials and Methods

Achieving the production of a desired hypernucleus largely depends on the choice of the exotic secondary beam that will be generated and directed at a secondary target. The Super-FRS separator's configuration is illustrated in Figure 1. Initially, a primary beam from the synchrotron impinges on a primary target, leading to the production of exotic fragments. The pre-separator then selects and purifies the desired exotic beam. This beam is transported to the focal plane FMF2 (pointed at with a pink arrow in Figure 1) of the main separator, where a secondary target is positioned for hypernuclei production. The subsequent segment of the main separator serves as a high-resolution spectrometer to analyze decay fragments from the mesonic-weak decay of the hypernucleus of interest. By configuring the fragment separator to focus on a particular momentum range or the magnetic rigidity of the decay fragment, the experiment can achieve a precise invariant mass measurement of the reconstructed hypernucleus. The FRS and Super-FRS spectrometers offer a momentum resolving power of $p/\Delta p = 1500$, enhancing measurement accuracy. To maximize experimental efficiency, a dedicated data-processing method was developed to predefine the optimal experimental settings needed to produce a specific exotic hypernucleus.

The optimization procedure followed in this study is similar to the one already reported in Ref. [31]. Nonetheless, the current analysis differed from the previous in one important step: the adjustment of the theoretical models of the hypernuclear production cross-section to the existing experimental data, as it is detailed in the next paragraphs.

The initial systematic study employed the EPAX model [32,33], which provides an energy-independent model for the fragmentation of cross-sections at relativistic energies during heavy-ion collisions. This phenomenological model uses a universal analytical formula derived from fragmentation reaction data of medium and heavy-ion projectiles [34]. It effectively estimates the production cross-sections of both exotic and stable nuclei for a wide range of collision systems. A comprehensive set of beam–target combinations was analyzed, establishing normalized yields of exotic beams per centimeter of production target length. Simulations covered all possible exotic isotopes from hydrogen to scandium, which were generated from stable isotopes up to ^{40}Ca. However, the maximum acceptable magnetic rigidities of the FRS (18 Tm) and Super-FRS (20 Tm) limit the usable isotopes at 2 *A*GeV.

To simulate the ion-optic transmission, the study integrated these yield estimations into the MOCADI code [35,36]. The MOCADI framework allows rare-isotope separator facilities, including the existing FRS and the future Super-FRS, to evaluate the availability of specific exotic secondary beams. This approach enables precise estimation of the transmission and yield of each potential exotic secondary beam using the Super-FRS system. The secondary

beam of interest, along with other exotic isotopes of similar magnetic rigidity, is transported from the production target to the focal plane FMF2 of the main separator of the Super-FRS, as depicted in Figure 1. At FMF2, a secondary target is set for hypernuclei production. The study also evaluates the secondary beam yield for each combination of beam and target species across varying target thicknesses. An optimization process within the MOCADI simulations was also developed to fine-tune the parameters of the ion-optical elements of the Super-FRS separator, aiming to maximize the intensity of the desired secondary beam at FMF2. This Monte Carlo study achieved systematic uncertainties of approximately 1%.

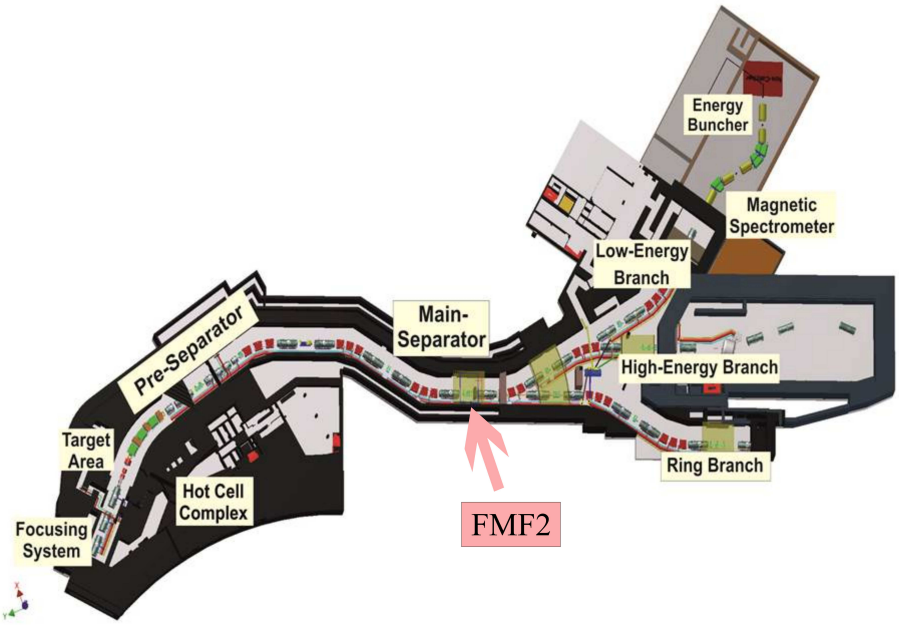

Figure 1. (Color online) Diagram of the Super-FRS fragment separator. The primary beam originating from the synchrotron, which collides with the primary target (in the target area) to generate the desired exotic beam, is inserted from the bottom left side of the image. The pre-separator section of the Super-FRS is responsible for selecting the exotic beam to ensure high quality. The following section of the main separator functions as a high-resolution forward spectrometer. At the focal plane FMF2 (marked with a pink arrow) of the main separator, a secondary target is positioned specifically for hypernuclei production. Image adapted from Ref. [4].

The theoretical model outlined in Ref. [37] was employed to analyze exotic hypernuclei production for each secondary beam of interest. This hybrid model combines the Dubna cascade model with a quark-gluon string model (DCM-QGSM) for simulating beam–target collisions [38] with a Fermi break-up model for describing spectator de-excitation [39]. Theoretical calculations included exotic beams from Li to Ne isotopes colliding with ^{12}C or ^{9}Be targets at 2 *A*GeV. Simulations were conducted with sufficient event counts to maintain a hypernuclei production cross-section uncertainty within 0.1 μb. To validate the model, theoretical predictions for ^{6}Li + ^{12}C collisions at 2 *A*GeV were compared against existing experimental data [19], showing good agreement. Because of this, the previously reported analysis [31] used the measured experimental cross-sections [19] and scaled the calculated ones with respect to the experimental values. However, in this study, only the theoretical cross-sections of the hypernuclear production are implemented without any modification.

Figure 2 shows the production cross-section of ${}^{6}_{\Lambda}$He, ${}^{9}_{\Lambda}$B, ${}^{9}_{\Lambda}$C, and ${}^{10}_{\Lambda}$C hypernuclei at 2 *A*GeV based on neutron and proton numbers of the exotic beam interacting with a ^{12}C target. This analysis helps identify the secondary beam isotope that maximizes each exotic hypernucleus production. However, the optimal scenario must also consider the feasibility of exotic beam production and adjustments for beam energy variations from 2 *A*GeV.

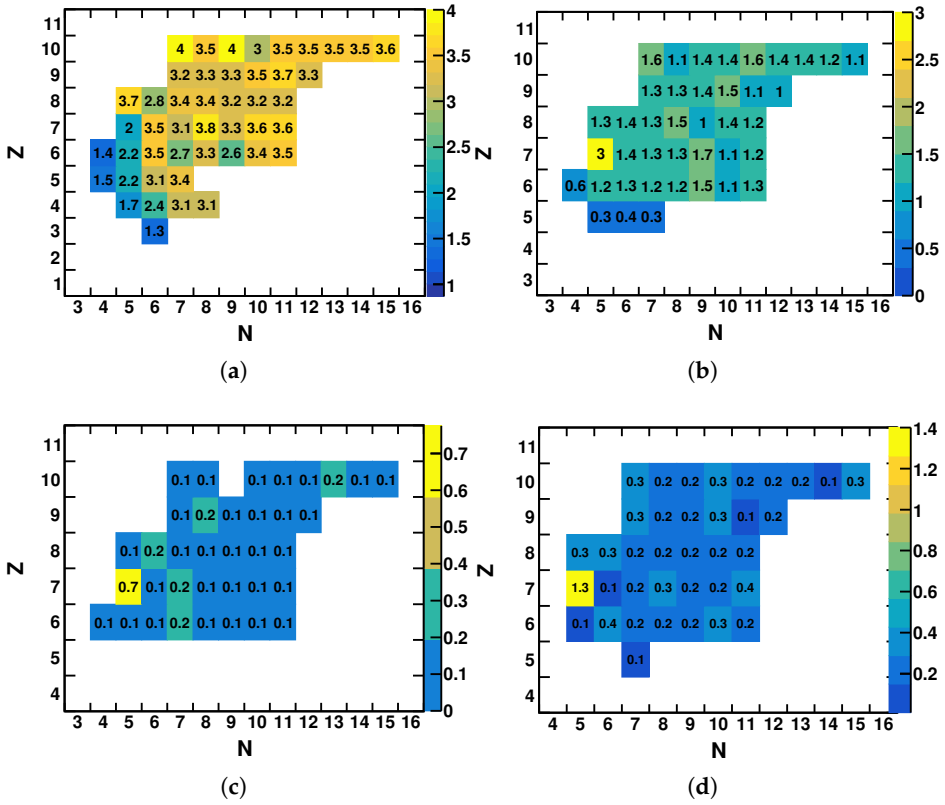

Figure 2. (Color online) Production cross-sections (in μb) for the hypernuclei (**a**) ${}^{6}_{\Lambda}$He, (**b**) ${}^{9}_{\Lambda}$B, (**c**) ${}^{9}_{\Lambda}$C, and (**d**) ${}^{10}_{\Lambda}$C, resulting from collisions of various exotic secondary beams ${}^{Z+N}$Z with a ^{12}C target at 2 *A*GeV. The systematic uncertainty of the cross-section measurements is approximately 0.1 μb.

The study applied a parametrization method [40] to adjust the theoretical calculations according to the exotic beam's kinetic energy, using the pp $\rightarrow$ pK$^{+}\Lambda$ cross-section data [41] for scaling. For example, reducing the beam energy to 1.9 *A*GeV or 1.8 *A*GeV results in 73% or 46% reductions in hypernuclei production cross-sections, respectively.

A multivariate dataset was constructed to optimize the experimental parameters for hypernucleus production. This dataset consolidates the theoretical and simulation results, including the optimal primary beam, production target, its thickness, and the ideal exotic secondary beam for each specific hypernucleus. Nevertheless, it is not feasible to directly visualize the multivariate dataset and identify the best case by simply compiling all possible combinations of isotopes species. An optimization procedure was implemented to find the optimal solution.

During the analysis, all possible secondary beam combinations with beryllium or carbon targets were considered in the theoretical calculations of hypernuclei production. The procedure selected the appropriate secondary beam to determine the optimal conditions of the Super-FRS, allowing the calculation of the hypernuclear yield per second for a 4 centimeter secondary production target. This target thickness was chosen to match the experimental conditions used in previous HypHI experiments. The estimated hypernuclear yield incorporates experimental efficiency from ion-optical transmission and an exotic beam intensity derived from a primary beam of 5×10^{9} ions/s. Additionally, a simpler case with a stable beam for hypernuclei production was included, using an intensity of 10^{7} ions/s to estimate the yield per second.

To solve the optimization problem, a cost function was defined considering several variables and parameters. The goal was to find the optimal set that maximizes or minimizes the cost function. The cost function is as follows:

$$F_{\alpha,\beta}(C, E, T, I) = \alpha C + \beta E - \gamma T + \delta I \quad (1)$$

where C, E, T, and I represent the hypernuclear yield, secondary beam energy, production target thickness, and intensity of the secondary beam of interest, respectively. The coefficients α, β, γ, and δ are weight factors that connect these variables. The coefficient δ for intensity was set to $1/2$ to ensure numerical stability during convergence. Additionally, the sum of the squared weights is constrained to 1, $\alpha^2 + \beta^2 + \gamma^2 + \delta^2 = 1$, with γ being determined as $\sqrt{3/4 - \alpha^2 - \beta^2}$. This ensures that α and β lie within a circle of radius $\sqrt{3/4}$. The variables were normalized to the range [0, 1] to maintain the weight coefficients within a unit interval. α and β are set based on the desired weight assigned to each variable. This cost function is specifically designed to maximize the production of the hypernucleus of interest by optimizing the energy and intensity of the secondary beam while minimizing the primary production target thickness. The optimization of these secondary beam characteristics is strongly related to the combination of primary beam and target species.

The search for the maximum of the cost function is performed with fixed values for α and β to identify the optimal parameter set:

$$\underset{C,E,T,I}{\operatorname{argmax}}\{F_{\alpha,\beta}(C, E, T, I)\} \quad (2)$$

3. Results

The results can then be analyzed based on different values of α and β. Figure 3 presents the outcomes of the optimization for the ${}^{6}_{\Lambda}$He case with each point representing a possible optimal condition set. The best condition is determined using the maximax criterion, which is defined as shown below:

$$\underset{\alpha,\beta}{\operatorname{argmax}} \max_{C,E,T,I} \{F_{\alpha,\beta}(C, E, T, I)\} \quad (3)$$

The evolution of the variable set as a function of α and β is illustrated in Figure 3. The images display the optimal primary beam and target species (Figure 3a,b), the target thickness (Figure 3c), the secondary beam isotope (Figure 3d) and its energy (Figure 3e), and the resulting yield of ${}^{6}_{\Lambda}$He (Figure 3f) as functions of α and β. The parameters α and β are varied within the range $[-\sqrt{3/4}, \sqrt{3/4}]$, where negative values of α aim to minimize hypernuclear yield, and negative values of β aim to reduce the kinetic energy of the secondary beam. Calculating the optimal conditions within the weight limits is valuable, as it allows for the consideration of alternative decision criteria beyond the maximax approach presented in Equation (3). Notwithstanding, the global optimal conditions are obtained with α and β values represented with a red star in Figure 3.

For the case of ${}^{6}_{\Lambda}$He, the optimization procedure leads to the following experimental conditions: a primary beam of ^{20}Ne ions on a 2-centimeter ^{9}Be target, with a selected exotic beam of ^{17}F, which is transported to bombard a ^{12}C target. The intensity of the ^{17}F secondary beam is approximately 5.7×10^6 ions per second, assuming a primary beam intensity of 5×10^9 ions per second, which aligns with the expected intensity at the Super-FRS. Under these conditions, the ${}^{6}_{\Lambda}$He yield is approximately 1.35 hypernuclei per second for a 4-centimeter secondary target.

Another example is shown in Figure 4, which presents the optimal conditions (marked by a red star) to produce ${}^{9}_{\Lambda}$C. This experimental setup involves directing a ^{14}N primary beam onto a ^{9}Be target with a thickness of 5.5 cm. This interaction generates an exotic ^{12}N beam, which is then transported to strike a 4-centimeter ^{12}C target. Considering a primary beam intensity of 5×10^9 ions per second, the ^{12}N secondary beam achieves an intensity of

approximately 5.1×10^6 ions per second. Under these conditions, the hypernuclear yield is 0.25 ${}^{9}_{\Lambda}$C per second.

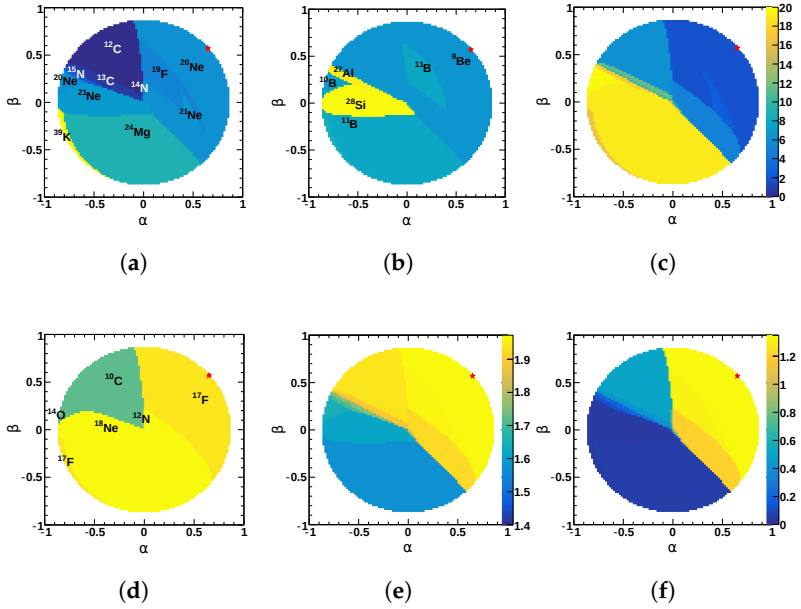

Figure 3. (Color online) Outcomes of the optimization of the multivariate dataset for the ${}^{6}_{\Lambda}$He case, showing the relationships between target thickness, beam energy, beam intensity, hypernuclear yield, exotic beam, primary beam, and target species. Images (**a**–**f**) display the evolution of the variables: the primary beam and target species, the target thickness in centimeters, the selected exotic beam species with its kinetic energy in *A*GeV, and the ${}^{6}_{\Lambda}$He yield per second. Each red star symbol indicates the position of the overall maximum within the α-β space.

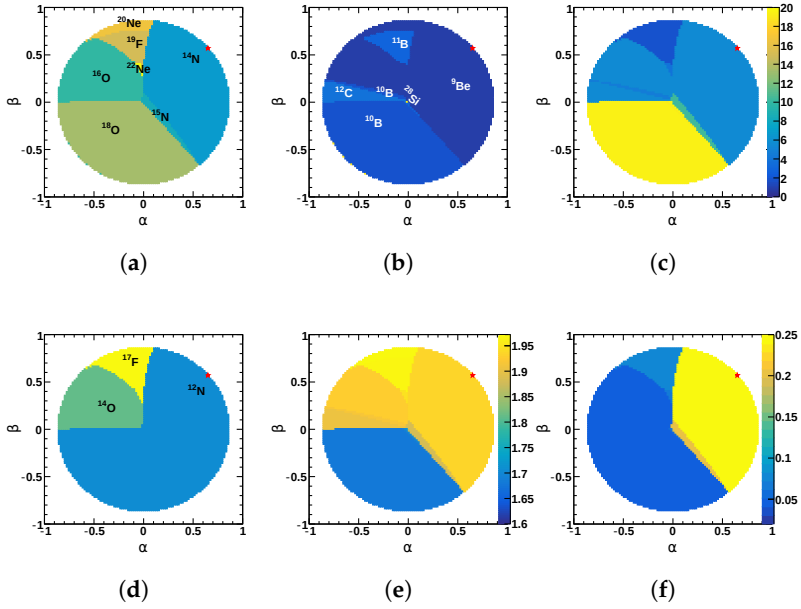

Figure 4. (Color online) Results of the multivariate dataset optimization for the ${}^{9}_{\Lambda}$C case, illustrating the interplay between target thickness, beam energy, beam intensity, hypernuclear yield, exotic beam, primary beam, and target species. Panels (**a**–**f**) depict the evolution of these variables, including the primary beam and target species, target thickness in centimeters, the selected exotic beam species along with its kinetic energy in *A*GeV, and the yield of ${}^{9}_{\Lambda}$C per second. Red star symbols mark the global maximum within the α-β parameter space.

The same approach can be applied to other hypernuclei. Table 1 summarizes the optimization results for Λ-hypernuclei up to carbon hypernuclei. It lists the necessary reaction for optimal exotic beam production, the target thickness, the selected exotic beam with its optimal kinetic energy and intensity, and the yield per second for each hypernucleus produced on a 4-centimeter ^{12}C target. These optimal experimental conditions will be valuable for designing future hypernuclear experiments at the Super-FRS facility.

Table 1. Summary of the optimization procedure results, covering all Λ-hypernuclei up to carbon isotopes. For each hypernucleus, the optimal experimental conditions are detailed, including the reaction needed to generate the exotic beam, the target thickness, the chosen exotic beam for hypernuclei production on a 4-centimeter ^{12}C target, as well as the exotic beam kinetic energy, the intensity, and the achieved hypernuclear yield.

	Reaction	Target (cm)	2nd Beam	E_k (*A*GeV)	*I* (10^6/s)	Yield (/s)
$^{2}_{\Lambda}$n	^{27}Al + ^{10}B	9	^{19}O	1.82	5.2	0.06
$^{3}_{\Lambda}$n	^{20}Ne + ^{9}Be	2	^{17}F	1.97	5.7	0.71
$^{4}_{\Lambda}$n	^{20}Ne + ^{9}Be	2	^{17}F	1.97	5.7	0.36
$^{5}_{\Lambda}$n	^{20}Ne + ^{9}Be	2	^{17}F	1.97	5.7	0.10
$^{6}_{\Lambda}$n	^{23}Na + ^{11}B	15.5	^{12}B	1.79	11	0.06
$^{3}_{\Lambda}$H	^{20}Ne + ^{9}Be	2	^{17}F	1.97	5.7	1.49
$^{4}_{\Lambda}$H	^{20}Ne + ^{9}Be	2	^{17}F	1.97	5.7	1.29
$^{5}_{\Lambda}$H	^{20}Ne + ^{9}Be	2	^{17}F	1.97	5.7	1.00
$^{6}_{\Lambda}$H	^{20}Ne + ^{9}Be	2	^{17}F	1.97	5.7	0.50
$^{7}_{\Lambda}$H	^{20}Ne + ^{9}Be	2	^{17}F	1.97	5.7	0.18
$^{8}_{\Lambda}$H	^{23}Na + ^{11}B	15.5	^{12}B	1.79	11	0.08
$^{3}_{\Lambda}$He	^{14}N + ^{9}Be	5.5	^{12}N	1.94	5.1	0.58
$^{4}_{\Lambda}$He	^{20}Ne + ^{9}Be	2	^{17}F	1.97	5.7	1.24
$^{5}_{\Lambda}$He	^{20}Ne + ^{9}Be	2	^{17}F	1.97	5.7	1.56
$^{6}_{\Lambda}$He	^{20}Ne + ^{9}Be	2	^{17}F	1.97	5.7	1.35
$^{7}_{\Lambda}$He	^{20}Ne + ^{9}Be	2	^{17}F	1.97	5.7	1.01
$^{8}_{\Lambda}$He	^{20}Ne + ^{9}Be	2	^{17}F	1.97	5.7	0.50
$^{9}_{\Lambda}$He	^{23}Na + ^{11}B	15.5	^{12}B	1.79	11	0.25
$^{4}_{\Lambda}$Li	^{20}Ne + ^{9}Be	2	^{17}F	1.97	5.7	0.39
$^{5}_{\Lambda}$Li	^{20}Ne + ^{9}Be	2	^{17}F	1.97	5.7	0.74
$^{6}_{\Lambda}$Li	^{20}Ne + ^{9}Be	2	^{17}F	1.97	5.7	1.29
$^{7}_{\Lambda}$Li	^{20}Ne + ^{9}Be	2	^{17}F	1.97	5.7	1.49
$^{8}_{\Lambda}$Li	^{20}Ne + ^{9}Be	2	^{17}F	1.97	5.7	1.26
$^{9}_{\Lambda}$Li	^{16}O + ^{9}Be	5.5	^{14}O	1.93	5.5	0.74
$^{10}_{\Lambda}$Li	^{23}Na + ^{11}B	15.5	^{12}B	1.79	11	0.34
$^{5}_{\Lambda}$Be	^{14}N + ^{9}Be	5.5	^{12}N	1.94	5.1	0.20
$^{6}_{\Lambda}$Be	^{14}N + ^{9}Be	5.5	^{12}N	1.94	5.1	0.61
$^{7}_{\Lambda}$Be	^{14}N + ^{9}Be	5.5	^{12}N	1.94	5.1	1.24
$^{8}_{\Lambda}$Be	^{20}Ne + ^{9}Be	2	^{17}F	1.97	5.7	1.25
$^{9}_{\Lambda}$Be	^{20}Ne + ^{9}Be	2	^{17}F	1.97	5.7	1.29
$^{10}_{\Lambda}$Be	^{20}Ne + ^{9}Be	2	^{17}F	1.97	5.7	0.92
$^{11}_{\Lambda}$Be	^{20}Ne + ^{9}Be	5	^{18}Ne	1.92	5.0	0.16
$^{7}_{\Lambda}$B	^{14}N + ^{9}Be	5.5	^{12}N	1.94	5.1	0.22
$^{8}_{\Lambda}$B	^{14}N + ^{9}Be	5.5	^{12}N	1.94	5.1	0.88
$^{9}_{\Lambda}$B	^{14}N + ^{9}Be	5.5	^{12}N	1.94	5.1	1.12
$^{10}_{\Lambda}$B	^{14}N + ^{9}Be	5.5	^{12}N	1.94	5.1	0.82
$^{11}_{\Lambda}$B	^{20}Ne + ^{9}Be	2	^{17}F	1.97	5.7	0.44

Table 1. *Cont.*

	Reaction	Target (cm)	2nd Beam	E_k (*A*GeV)	*I* (10^6/s)	Yield (/s)
${}^{8}_{\Lambda}$C	^{14}N + ^{9}Be	5.5	^{12}N	1.94	5.1	0.07
${}^{9}_{\Lambda}$C	^{14}N + ^{9}Be	5.5	^{12}N	1.94	5.1	0.25
${}^{10}_{\Lambda}$C	^{14}N + ^{9}Be	5.5	^{12}N	1.94	5.1	0.49
${}^{11}_{\Lambda}$C	^{14}N + ^{9}Be	5.5	^{12}N	1.94	5.1	0.29

4. Discussion

A systematic approach was developed to identify the optimal experimental conditions for producing exotic hypernuclei within the Super-FRS fragment separator at the new FAIR facility, where future hypernuclear spectroscopy experiments will be conducted [31]. This optimization process integrates results from multiple theoretical models, including predictions of hypernuclei and exotic beam production through the fragmentation of the primary beam on the production target. It also incorporates Monte Carlo simulations of beam transport to estimate the experimental efficiency of the separator. These efficiencies correspond to the transmission from the secondary beam production site to the experimental area, where both hypernuclei production and spectroscopy will occur.

The optimization method combines these diverse inputs to determine the best conditions for any hypernucleus under consideration by maximizing the cost function. Specifically, for the ${}^{6}_{\Lambda}$He (${}^{9}_{\Lambda}$C) hypernucleus, the optimal configuration involves using a ^{17}F (^{12}N) secondary beam derived from the fragmentation of a ^{20}Ne (^{14}N) primary beam on a ^{9}Be target. This setup could produce approximately 1.35 ${}^{6}_{\Lambda}$He (0.25 ${}^{9}_{\Lambda}$C) nuclei per second on a 4-centimeter ^{12}C target with an estimated production cross-section of 3.3 (0.7) μb. Given these conditions and the efficiency observed in previous experiments [17], around 11.700 (2.100) hypernuclei per day are expected.

The optimization process was extended to cover all hypernuclei up to carbon isotopes, providing valuable insights for future experiments on both proton-rich and neutron-rich hypernuclei. These results were achieved using a specific quasi-convex combination of the variables involved in the optimization. However, alternative approaches remain to be explored, particularly regarding the weight definitions in the cost function. Additionally, while the maximax criterion was applied in this study, other decision-making strategies could be considered to adjust the weights, offering new perspectives on the dataset.

Author Contributions: Conceptualization, S.E. and C.R.; methodology, C.R.; software, C.R.; validation, C.R.; formal analysis, C.R.; investigation, C.R.; resources, C.R.; data curation, C.R.; writing—original draft preparation, S.E.; writing—review and editing, S.E. and C.R.; visualization, S.E. and C.R.; supervision, C.R.; project administration, C.R.; funding acquisition, C.R. All authors have read and agreed to the published version of the manuscript.

Funding: This research was supported by the HypHI project, funded by the Helmholtz Association as the Helmholtz-University Young Investigators Group VH-NG-239 at GSI, as well as by the German Research Foundation (DFG) under contract number SA 1696/1-1 and the EU FP7 HadronPhysics-2 SPHERE. Additional support was provided by the University of Castilla-La Mancha through the co-funded program "Ayudas para estancias de investigadores invitados en la UCLM para el año 2015" and FEDER 2014-2020. This work is also funded by the grants 2019-T1/TIC-13194 and 2023-5A/TIC-28925 of the program "Atracción de Talento Investigador" of the Comunidad de Madrid, and by the fund PID2022-140162NB-I00 of "Proyectos I+D+i 2022" of the Agencia Estatal de Investigación (Gobierno de España).

Institutional Review Board Statement: Not applicable.

Informed Consent Statement: Not applicable.

Data Availability Statement: The original contributions presented in this study are included in the article. Further inquiries can be directed to the corresponding author.

Acknowledgments: Part of this work was performed using the HIMSTER high-performance computing infrastructure provided by the Helmholtz-Institute Mainz. We would also like to express our gratitude to A. Botvina, H. Geissel, T. Saito, and C. Scheidenberger for their valuable discussions and insights.

Conflicts of Interest: The authors declare no conflicts of interest. The funders had no role in the design of the study; in the collection, analyses, or interpretation of data; in the writing of the manuscript; or in the decision to publish the results.

References

1. Koch, P.; Müller, B.; Rafelski, J. Strangeness in relativistic heavy ion collisions. *Phys. Rep.* **1986**, *142*, 167–262. [CrossRef]
2. Margetis, S.; Safarík, K.; Villalobos Baillie, O. Strangeness Production in Heavy-Ion Collisions. *Annu. Rev. Nucl. Part. Sci.* **2000**, *50*, 299–342. [CrossRef]
3. Tamura, H. Baryon-baryon interactions with strangeness studied from hypernuclei. *Nucl. Phys. A* **2005**, *752*, 155–164.
4. GSI Helmholtz Centre for Heavy Ion Research. Available online: https://www.gsi.de (accessed on 1 February 2025).
5. FAIR Facility for Antiproton and Ion Research in Europe. Available online: https://fair-center.eu (accessed on 1 February 2025).
6. Blasche, K.; Bohne, D.; Franzke, B.; Prange, H. The SIS Heavy Ion Synchrotron Project. *IEEE Trans. Nucl. Sci.* **1985**, *32*, 2657–2661. [CrossRef]
7. Blasche, K.; Prange, H.; Eickhoff, H.; Steiner, R.; Böhne, D.; Franczak, B.; Franzke, B. Status of the SIS/ESR-facility at Gsi Darmstadt. *Part. Accel.* **1990**, *32*, 83–90.
8. Armbruster, P.; Clerc, H.; Dufour, J.P.; Franczak, B.; Geissel, H.; Hanelt, E.; Klepper, O.; Langenbeck, B.; Münzenberg, G.; Nickel, F.; et al. The projectile-fragment separator at the Darmstadt SIS/ESR facility. *AIP Conf. Proc.* **1987**, *164*, 839–844. [CrossRef]
9. Geissel, H.; Armbruster, P.; Behr, K.; Brünle, A.; Burkard, K.; Chen, M.; Folger, H.; Franczak, B.; Keller, H.; Klepper, O.; et al. The GSI projectile fragment separator (FRS): A versatile magnetic system for relativistic heavy ions. *Nucl. Instrum. Meth. B* **1992**, *70*, 286–297. [CrossRef]
10. Geissel, H.; Weick, H.; Winkler, M.; Münzenberg, G.; Chichkine, V.; Yavor, M.; Aumann, T.; Behr, K.; Böhmer, M.; Brünle, A.; et al. The Super-FRS project at GSI. *Nucl. Instrum. Meth. B* **2003**, *204*, 71–85.
11. Hashimoto, O.; Tamura, H. Spectroscopy of Λ hypernuclei. *Prog. Part. Nucl. Phys.* **2006**, *57*, 564–653. [CrossRef]
12. Botta, E.; Bressani, T.; Garbarino, G. Strangeness nuclear physics: A critical review on selected topics. *Eur. Phys. J. A* **2012**, *48*, 41. [CrossRef]
13. Feliciello, A.; Nagae, T. Experimental review of hypernuclear physics: Recent achievements and future perspectives. *Rep. Prog. Phys.* **2015**, *78*, 096301. [CrossRef] [PubMed]
14. Nield, K.J.; Bowen, T.; Cable, G.D.; DeLise, D.A.; Jenkins, E.W.; Kalbach, R.M.; Noggle, R.C.; Pifer, A.E. Production of hypernuclei in a 2.1 GeV/nucleon oxygen beam. *Phys. Rev. C* **1976**, *13*, 1263–1266. [CrossRef]
15. Abdurakhimov, A.; Aksinenko, V.; Anikina, M.; Avramenko, S.; Bannik, B.; Butenko, V.; Glagoleva, N.; Golokhvastov, A.; Grachev, A.; Dementiev, E.; et al. Experimental study of relativistic hypernuclei using the HYBS-spectrometer. *Nuov. Cim. A* **1989**, *102*, 645–652. [CrossRef]
16. Avramenko, S.; Aksinenko, V.; Anikina, M.; Bannik, B.; Belikov, Y.; Butenko, V.; Drozdov, V.; Gajevski, K.; Galperin, A.; Glagoleva, N.; et al. A study of the production and lifetime of the lightest relativistic hypernuclei. *Nucl. Phys. A* **1992**, *547*, 95–100. [CrossRef]
17. Rappold, C.; Kim, E.; Nakajima, D.; Saito, T.; Bertini, O.; Bianchin, S.; Bozkurt, V.; Kavatsyuk, M.; Ma, Y.; Maas, F.; et al. Hypernuclear spectroscopy of products from ^{6}Li projectiles on a carbon target at 2 *A*GeV. *Nucl. Phys. A* **2013**, *913*, 170–184. [CrossRef]
18. Rappold, C.; Kim, E.; Saito, T.R.; Bertini, O.; Bianchin, S.; Bozkurt, V.; Kavatsyuk, M.; Ma, Y.; Maas, F.; Minami, S.; et al. Search for evidence of ${}^{3}_{\Lambda}n$ by observing $d + \pi^-$ and $t + \pi^-$ final states in the reaction of ^{6}Li+^{12}C at 2*A* GeV. *Phys. Rev. C* **2013**, *88*, 041001. [CrossRef]
19. Rappold, C.; Saito, T.; Bertini, O.; Bianchin, S.; Bozkurt, V.; Kim, E.; Kavatsyuk, M.; Ma, Y.; Maas, F.; Minami, S.; et al. Hypernuclear production cross-section in the reaction of 6Li + 12C at 2 A GeV. *Phys. Lett. B* **2015**, *747*, 129–134. [CrossRef]
20. Miyagawa, K.; Kamada, H.; Glöckle, W.; Stoks, V. Properties of the bound Λ(Σ)NN system and hyperon-nucleon interactions. *Phys. Rev. C* **1995**, *51*, 2905–2913. [CrossRef]
21. Gal, A.; Garcilazo, H. Is there a bound nΛ3? *Phys. Lett. B* **2014**, *736*, 93–97. [CrossRef]

22. Hiyama, E.; Ohnishi, S.; Gibson, B.F.; Rijken, T.A. Three-body structure of the $nn\Lambda$ system with $\Lambda N - \Sigma N$ coupling. *Phys. Rev. C* **2014**, *89*, 061302. [CrossRef]
23. Ando, S.I.; Raha, U.; Oh, Y. Investigation of the nnΛ bound state in pionless effective theory. *Phys. Rev. C* **2015**, *92*, 024325. [CrossRef]
24. Richard, J.M.; Wang, Q.; Zhao, Q. Lightest neutral hypernuclei with strangeness -1 and -2. *Phys. Rev. C* **2015**, *91*, 014003. [CrossRef]
25. Saito, T.R.; Dou, W.; Drozd, V.; Ekawa, H.; Escrig, S.; He, Y.; Kalantar-Nayestanaki, N.; Kasagi, A.; Kavatsyuk, M.; Liu, E.; et al. New directions in hypernuclear physics. *Nat. Rev. Phys.* **2021**, *3*, 803–813. [CrossRef]
26. Escrig, S. Status of the WASA-FRS HypHI Experiment: Study of Light Hypernuclei at GSI-FAIR. *Acta Phys. Pol. B Proc. Suppl.* **2024**, *17*, 3-A19. [CrossRef]
27. Saito, T.; Achenbach, P.; Alfaki, H.A.; Amjad, F.; Armstrong, M.; Behr, K.H.; Benlliure, J.; Brencic, Z.; Dickel, T.; Drozd, V.; et al. The WASA-FRS project at GSI and its perspective. *Nucl. Instrum. Meth. B* **2023**, *542*, 22–25. [CrossRef]
28. Acharya, S.; Adamová, D.; Adler, A.; Aglieri Rinella, G.; Agnello, M.; Agrawal, N.; Ahammed, Z.; Ahmad, S.; Ahn, S.U.; Ahuja, I.; et al. Measurement of the Lifetime and Λ Separation Energy of ${}^{3}_{\Lambda}$H. *Phys. Rev. Lett.* **2023**, *131*, 102302. [CrossRef]
29. Adam, J.; Adamczyk, L.; Adams, J.R.; Adkins, J.K.; Agakishiev, G.; Aggarwal, M.M.; Ahammed, Z.; Alekseev, I.; Anderson, D.M.; Aparin, A.; et al. Measurement of the mass difference and the binding energy of the hypertriton and antihypertriton. *Nat. Phys.* **2020**, *16*, 409–412. [CrossRef]
30. Bargholtz, C.; Bashkanov, M.; Berłowski, M.; Bondar, A.; Bogoslawsky, D.; Brodowski, W.; Brudvik, J.; Calén, H.; Capellaro, F.; Chilingarov, A.; et al. The WASA detector facility at CELSIUS. *Nucl. Instrum. Meth. A* **2008**, *594*, 339–350. [CrossRef]
31. Rappold, C.; López-Fidalgo, J. Examination of experimental conditions for the production of proton-rich and neutron-rich hypernuclei. *Phys. Rev. C* **2016**, *94*, 044616. [CrossRef]
32. Sümmerer, K.; Brüchle, W.; Morrissey, D.J.; Schädel, M.; Szweryn, B.; Weifan, Y. Target fragmentation of Au and Th by 2.6 GeV protons. *Phys. Rev. C* **1990**, *42*, 2546–2561. [CrossRef]
33. Sümmerer, K.; Blank, B. Modified empirical parametrization of fragmentation cross sections. *Phys. Rev. C* **2000**, *61*, 034607. [CrossRef]
34. Sümmerer, K. Improved empirical parametrization of fragmentation cross sections. *Phys. Rev. C* **2012**, *86*, 014601. [CrossRef]
35. Iwasa, N.; Weick, H.; Geissel, H. New features of the Monte-Carlo code MOCADI. *Nucl. Instrum. Meth. B* **2011**, *269*, 752–758. [CrossRef]
36. Iwasa, N.; Geissel, H.; Münzenberg, G.; Scheidenberger, C.; Schwab, T.; Wollnik, H. MOCADI, a universal Monte Carlo code for the transport of heavy ions through matter within ion-optical systems. *Nucl. Instrum. Meth. B* **1997**, *126*, 284–289.
37. Buyukcizmeci, N.; Botvina, A.S.; Pochodzalla, J.; Bleicher, M. Mechanisms for the production of hypernuclei beyond the neutron and proton drip lines. *Phys. Rev. C* **2013**, *88*, 014611. [CrossRef]
38. Botvina, A.S.; Gudima, K.K.; Steinheimer, J.; Bleicher, M.; Mishustin, I.N. Production of spectator hypermatter in relativistic heavy-ion collisions. *Phys. Rev. C* **2011**, *84*, 064904. [CrossRef]
39. Botvina, A.S.; Pochodzalla, J. Production of hypernuclei in multifragmentation of nuclear spectator matter. *Phys. Rev. C* **2007**, *76*, 024909. [CrossRef]
40. Fäldt, G.; Wilkin, C. Comparison of the near-threshold production of η-and K-mesons in proton-proton collisions. *Z. Phys. A* **1997**, *357*, 241–243. [CrossRef]
41. The COSY-TOF Collaboration; Abdel-Bary, M.; Abdel-Samad, S.; Brinkmann, K.T.; Clement, H.; Dietrich, J.; Doroshkevich, E.; Dshemuchadse, S.; Ehrhardt, K.; Erhardt, A.; et al. Production of and hyperons in proton-proton collisions. *Eur. Phys. J. A* **2010**, *46*, 27–44. [CrossRef]